*minerals*

MDPI

*Article*

# Quantifying the Contribution and Mobility of In Situ-Produced Helium in He-Retentive Minerals: A Case Study of the Salla-Kuolajarvi Metasomatic Rocks (Russia)

**Maria Andreevna Gannibal [1,*], Andrey Evgenievich Gannibal [1], Arkadii Avenirovich Kalinin [1], Tatiana Vladimirovna Kaulina [1] and Vitalii Valentinovich Kolobov [2]**

[1] Geological Institute, Kola Science Center of the Russian Academy of Sciences, Fersman St. 14, 184209 Apatity, Russia; han_a_e@mail.ru (A.E.G.); a.kalinin@ksc.ru (A.A.K.); t.kaulina@ksc.ru (T.V.K.)
[2] Northern Energetics Research Centre, Kola Science Centre of the Russian Academy of Sciences, Akademgorodok 21a, 184209 Apatity, Russia; 1_i@mail.ru
* Correspondence: m.a.gannibal@gmail.com; Tel.: +7-9211578614

**Abstract:** An alternative approach to separating trapped and radiogenic helium, and assessing the mobility of the latter in He-retentive minerals implemented in the present work, has been developed on the basis of helium extraction patterns obtained via incremental heating of mineral samples. We used these data both to estimate helium mobility in concentrates of various ore minerals (pyrite, magnetite, and hematite) and to assess the contribution of in situ-produced $^4$He in the total helium budget. The rocks of uranium-ore and gold mineralization of the Salla-Kuolajarvi belt (northern Karelia, Fennoscandian Shield) were used as test materials for the new approach. The method allowed such parameters as diffusivity, activation energy, closure temperature, and the contribution of the trapped helium to be obtained for all samples. The latter was used for the correction of apparent U-Th-He bulk ages. The interpretation of the calculated values was performed taking into account the closure temperatures of the U-Th-He system, as well as the peculiarities of each individual sample.

**Keywords:** uranium; thorium; helium; U-Th-He system; closure temperature; diffusion; metasomatic rocks; accessory minerals

check for updates

**Citation:** Gannibal, M.A.; Gannibal, A.E.; Kalinin, A.A.; Kaulina, T.V.; Kolobov, V.V. Quantifying the Contribution and Mobility of In Situ-Produced Helium in He-Retentive Minerals: A Case Study of the Salla-Kuolajarvi Metasomatic Rocks (Russia). *Minerals* **2024**, *14*, 1252. https://doi.org/10.3390/min14121252

Academic Editors: Ruxin Ding, Honghua Lv and Rong Yang

Received: 4 November 2024
Revised: 6 December 2024
Accepted: 7 December 2024
Published: 9 December 2024

**Copyright:** © 2024 by the authors. Licensee MDPI, Basel, Switzerland. This article is an open access article distributed under the terms and conditions of the Creative Commons Attribution (CC BY) license (https://creativecommons.org/licenses/by/4.0/).

## 1. Introduction

The U-Th-He system has proven a useful thermochronological tool over past decades, starting with the initial work by Zeitler [1] that rekindled interest in this particular dating method, indicating that some minerals are capable of retaining quantitative helium below a specific closure temperature. By now, the method has a well-developed procedure, owing, first of all, to the numerous studies of apatite and, to a lesser extent, to other He-retentive minerals (see, e.g., the reviews [2–4] and references therein). The adopted procedures generally involve small samples of one or a few grains used for determining both parent and daughter element concentrations, a more or less established heating protocol, and α-emission corrections. Though it is not always the case, it is often implied that the samples better be idiomorphic crystals, or else the result may turn out questionable. Another prerequisite is that the mineral grains should be free from inclusions, both fluid and solid. These constraints largely discard many potential research objects as unfit, for although idiomorphic crystals are not too hard to come by, those are also supposed to belong to a certain group of mineral species, providing the quantitative retaining of the radiogenic helium below the closure temperature that should be well above the values typical of surface conditions. In addition, fluid inclusions are rather ubiquitous in most geological settings.

To get around the constraints placed on the material by the dating procedure, one should deal with actual complications which imposed these constraints in the first place. Provided that the samples are represented by the minerals separated from the commonplace

rocks, there are two major features that would corrupt correct dating: (i) the retention ability of individual samples for helium may vary in a rather wide range because of the diversity of genetic and petrographic features; it would hardly be correct to adopt diffusion parameters obtained for one specific sample as a common characteristics of the given mineral; (ii) some amount of helium, hosted by fluid inclusions, is to be expected. Other material-related issues affecting apparent U-Th-He age, such as, e.g., excess helium, implanted from coexisting U- or Th-rich phase or α-particles lost directly during decay, would, of course, be present also, however, those are addressed elsewhere [5–7] and left beyond the scope of this contribution. The strategy, therefore, is to identify and eliminate the bulk of the excess helium, quantify the mineral retaining ability for radiogenic helium best as possible, and devise relevant correction procedures.

To achieve that goal, we have chosen the method of the incremental heating (hereafter IH), as termed in [8]. The essence of the method is recording a flux of a noble gas isotope, emitted from the investigated sample as a result of the linear increase in the sample temperature. It was used quite widely by founder members of the Russian school of noble gas geochemical and geochronological research in the early sixties of the last century [9,10]. Incremental heating was in high demand back then because of its ability to reflect, on a qualitative level, the behavior of the major noble gas isotopes in the rocks, which could be used to deduce the value of the latter for specific geochemical and chronological purposes.

The decline of the incremental heating method could be attributed largely to qualitative nature of the results. The then-present technology, especially the deficit of computing tools, offered very little opportunity for quantifying incremental heating patterns. The little that could have been done had to be very time- and resource-consuming. On the other hand, roughly at the same time, Fechtig and Kalbitzer [11] offered a methodological protocol for determining noble gas diffusivity in the crystalline substance from the stepwise heating experiments. The procedure, though rather time-consuming, involved quite an easy-to-do experimental approach and simple calculations and was, therefore, used for years ahead.

However, as the method indeed provided information about the behavior of the noble gases in the natural (imperfect) crystalline media, it was bound to be revisited. Thus, the work in [12] addressed differences between slow and rapid He release patterns to evaluate the rate of helium exchange between fluid inclusions and the mineral matrix. The research carried out in the aforementioned contribution [8] presented the model for He diffusion from riebeckite, again, based on the incremental heating curve.

The gas extraction procedure termed Continuous Ramped Heating (CRH) was suggested and started being vigorously developed quite recently [13–15]. CRH actually represented a selfsame IH carried out with the helium flux spreading into the closed mass-spectrometer camera to yield the cumulative curve so that, in the end of the run, the amount of helium released could be quantified. Such a protocol was proposed for revealing complications in helium diffusion pattern prior to thermochronometric research so as to discard unsuitable material before putting too much effort into it.

Thus, the goal of this contribution is to use the IH patterns to distinguish between helium of different origin and, at the same time, to quantify the mobility of the radiogenic fraction.

It should be noted that the proposed method, if proven reliable, can be applied to a far wider range of problems related to noble gases: separating in situ and trapped components, and assessing the retention of the former based on the actual mobility parameters, may also be of use in reconstructing characteristics of the trapped component which is quite common objective for the research in isotopic geochemistry [16]. Here, we analyzed ore minerals (pyrite, magnetite, and hematite) and amphibole from metasomatic rocks of the Salla-Kuolajarvi area (Russia), where the geological situation and thermochronological evolution of rocks had been studied previously.

## 2. Object of Research

The Salla-Kuolajarvi belt is located in the north-eastern part of the Fennoscandian Shield in the Karelian craton at the boundary with the Belomorian mobile belt (Figure 1A). The belt extends from south to north for 120 km, and it is 60 km wide. The eastern part of the belt is in Russia, and its western part is in Finland.

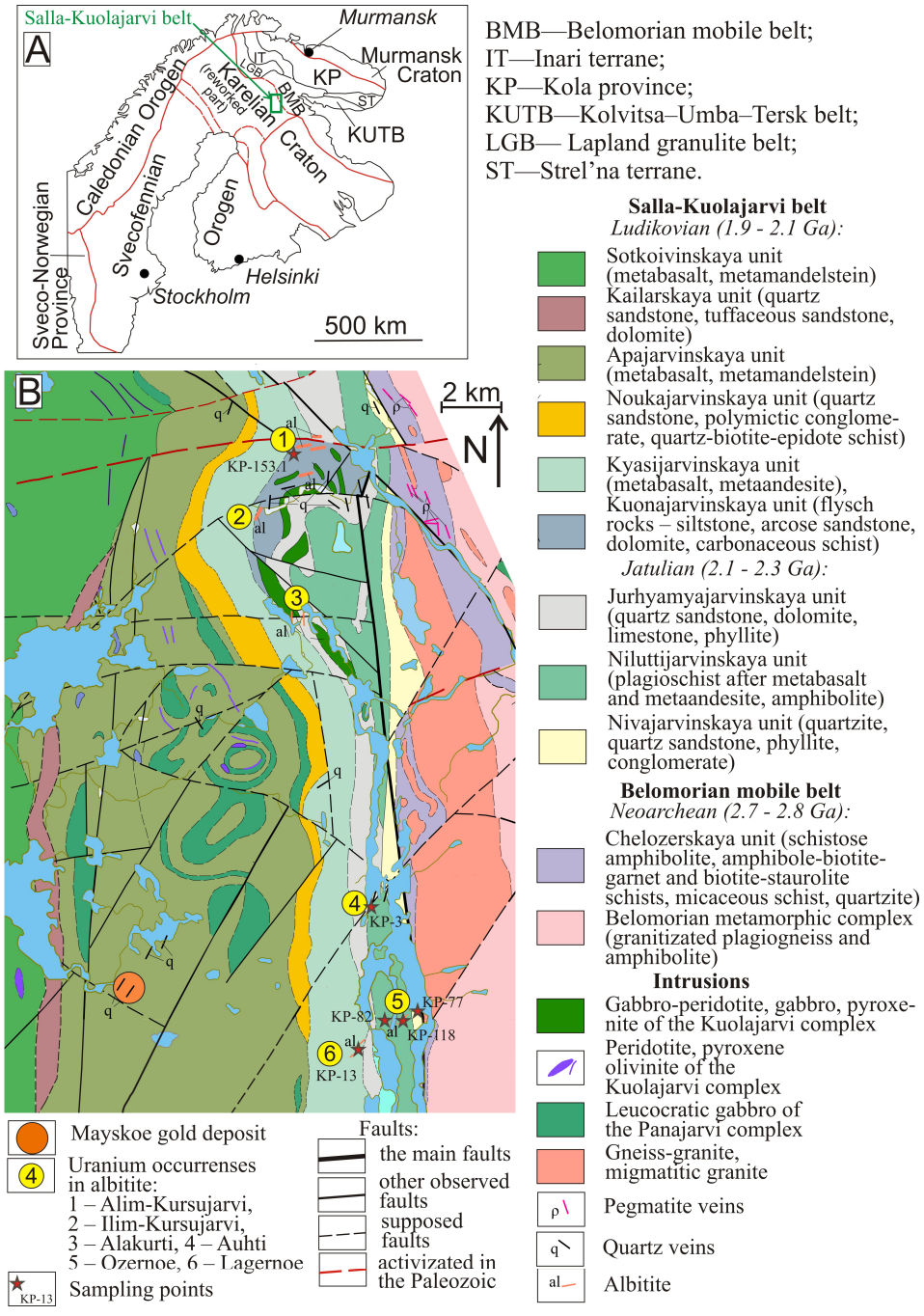


**Figure 1.** Position of the Salla-Kuolajarvi belt in the tectonic map of the Fennoscandian Shield (**A**) and a schematic geological map of the eastern part of the Salla-Kuolajarvi belt (**B**) (adapted after [17]).

The belt is of asymmetric structure. The eastern part has a simple cross-section with rock sequences dipping west at an angle of 70° (in the flank) to 10° (in the center of the belt). In the western part of the belt (not shown in Figure 1), the metamorphosed sedimentary and volcanic sequences are highly folded, faulted, and affected by granite intrusions [18].

Volcanic-sedimentary rocks of the Salla-Kuolajarvi belt formed in Jatulian (2.3–2.1 Ga) and Ludikovian (2.1–1.92 Ga), while older rocks are known only in the western part of the belt [19]. The geological section is composed of mafic metavolcanics, alternating with metasedimentary terrigenous rocks and dolomites (Figure 1B).

Volcanic-sedimentary complexes were greenschist metamorphosed during the collision events at 1.95–1.75 Ga [20], and in the eastern marginal part of the belt conditions of metamorphism reached the amphibolite facies [21].

A small gold deposit Mayskoe, composed of two gold-mineralized quartz veins in basalt, is located in the central part of the belt. A series of volcanogenic massive sulfide pyrite-magnetite-chalcopyrite prospects and albitite occurrences with uranium mineralization is located at the eastern flank of the Salla-Kuolajarvi belt (Figure 1B). Some of these albitite occurrences contain Au, Se, Te, Mo, and Re mineralization [17]. Albitite forms zonal lenses up to 10 m thick and 10–90 m long, and the albitite lenses cross general strike of the wall rocks. Albitite may be hosted by different metasedimentary, metavolcanic, or intrusive rocks (Figure 1B). The texture of sulfide and oxide mineralization is disseminated, veinlet-disseminated, or nested.

Uranium mineralization in albitite, as described in [21,22], is of long and multi-stage hydrothermal-metasomatic genesis. Three stages of evolution of mineralized albitite were defined with isotope geochronology [21,22]:

- 1.75 Ga—the age of albitite (U-Pb—rutile; Sm-Nd—whole rock and minerals, Rb-Sr—whole rock and minerals), the lower temperature limit of albitite formation was 400–450 °C;
- 1.62 Ga—formation of chlorite and carbonate metasomatic rocks after albitite and deposition of uraninite (electron microprobe dating of uraninite in albitite from Ozernoe, Rb-Sr—whole rock and minerals from Mayskoe deposit [23]) at a temperature not lower than 300–350 °C;
- 385 Ma—hydrothermal activity, caused by alkaline-carbonate intrusions: recrystallization of uranium minerals (U-Pb—brannerite).

## 3. Materials and Methods

### *3.1. Materials*

The investigated rocks of the Salla-Kuolajarvi belt and minerals separated are listed and described in Table 1. The images of thin sections and polished sections are presented in Figure 2.

**Table 1.** Samples.

| Sample No. | Ore Occurrence, Sample Coordinates | Rock/Mineral | Rock Description |
|---|---|---|---|
| KP-3 | Auhti<br>N 66°38.9′<br>E 29°51.8′ | Albitite with pyrite/<br>Pyrite | Medium-grained albitite composed of albite-oligiclase, quartz and carbonates (dolomite and calcite), contains nested-disseminated pyrite mineralization. |
| KP-13 | Lagernoe<br>N 66°36.7′<br>E 29°51.3′ | Biotite plagioschist/<br>Magnetite | Leucocratic banded fine-grained rock of plagioclase-quartzbiotite composition. Banding is caused by variable distribution of quartz grains. Magnetite forms regular dissemination of idiomorphic grains, those bands, which are rich in quartz, are poor in magnetite. |
| KP-77 | Ozernoe<br>N 66°37.1′<br>E 29°53.9′ | Albitite/<br>Hematite | Fine-grained rock composed mainly of albite-oligiclase, with rare quartz grains and sericite flakes, with hematite dissemination. |

**Table 1.** *Cont.*

| Sample No. | Ore Occurrence, Sample Coordinates | Rock/Mineral | Rock Description |
|---|---|---|---|
| KP-82 | Ozernoe<br>N 66°36.9′<br>E 29°52.5′ | Amphibolite/<br>Hornblende | Fine- to medium-grained rock, composed of plagioclase and hornblende. Amphibole crystals are oriented according to schistosity. The space between the amphibole grains is filled with plagioclase and quartz. |
| KP-118 | Ozernoe<br>N 66°37.0′<br>E 29°53.0′ | Albite-biotite rock/<br>Magnetite | Fine- to medium-grained rock, composed of albite-oligoclase, carbonates, and biotite. Magnetite is unevenly distributed, the bigger grains associate with clusters of biotite flakes. |
| KP-153.1 | Alim-Kursujarvi<br>N 66°46.3′<br>E 29°48.7′ | Magnetite-pyrite massive ore/Pyrite | Massive ore, composed of magnetite and pyrite, the space between the magnetite and pyrite grains is filled with carbonate, rare with chlorite and quartz. |

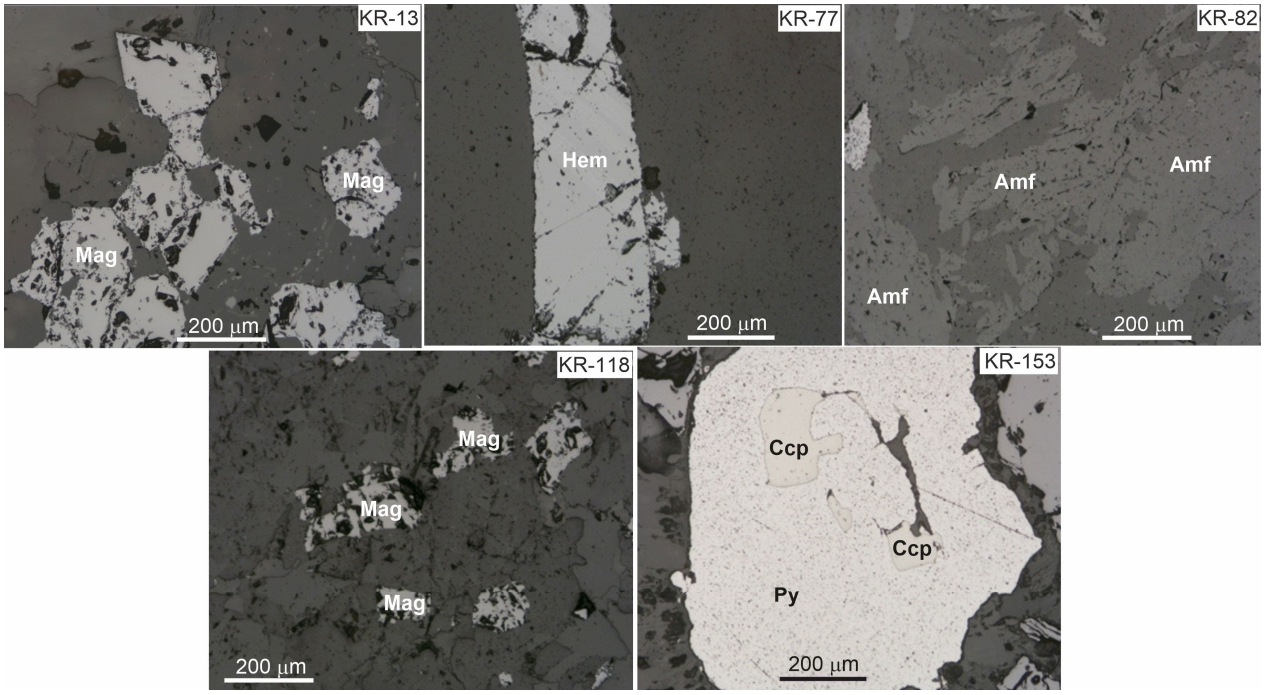


**Figure 2.** Images of the studied ore minerals in reflected light (polished sections). Mag—magnetite, Hem—hematite, Amf—amphibole, Py—pyrite, Ccp—chalcopyrite.

### *3.2. Methods*

Mineral separation was carried out in the separation laboratory of the Geological Institute of Kola Science Centre RAS according to the conventional procedure involving the multistage crushing and separation of minerals in heavy liquids by density, as well as using a roller electromagnet to separate the magnetic fraction. The separated minerals were subjected to a thorough refining procedure under a binocular microscope. The mineral composition of the obtained concentrates was confirmed by X-ray phase analysis. The sample particle sizes varied from 0.25 to 0.63 mm (when referred to as grains), while particle sizes of the ground sample were from ~$5 \times 10^{-3}$ to ~$5 \times 10^{-1}$ mm.

Thermal helium extraction from the samples during incremental heating runs was performed in a stainless-steel crucible heated by a resistance furnace up to ~1000–1100 °C. Samples of ~20 mg were loaded into the stainless steel cup, the top part of which was then crimped to prevent sample scattering. The crucible had a thick (20 mm) bottom with a thermocouple slot drilled out so that the head of the measuring K-type thermocouple was

within 2 mm from the inner surface of the crucible. The control experiments have shown that the temperature readings coincided within 2° with those measured directly in the sample and displayed no significant time lag. The linear heating was provided by a digital temperature controller.

Gases extracted from a mineral were admitted into the purification system. They passed through cold charcoal traps and Ti-Zr getters where chemically active gases and heavy noble gases were mostly removed; the residual gases (He and Ne) proceeded into the camera of the mass spectrometer and then pumped out, thus forming a constant flow through the camera. The intensity of $^4$He line was recorded using secondary electron multiplier.

To quantify the helium amount corresponding to the IH curve, we used the same heating protocol (heating rate and limiting temperature) as during IH runs. The released gas was accumulated within the inlet system and purified by the same means (cold charcoal traps and Ti-Zr getters). We also had an option of fusing the sample using a double-vacuum furnace with Mo heater, which would ensure the total amount of helium to be extracted, which, however, was used infrequently. In both cases, the purified gas extracted from the sample was admitted to the MS camera where the $^4$He amount was measured using a faraday cup in the static mode. Before and after each static experiment, the mass spectrometer was calibrated by the laboratory standard (peak-height method). The sensitivity for $^4$He was $3 \times 10^{-5}$ A torr$^{-1}$.

The magnetic sector mass spectrometer (MI 1201) was used for measurements of both flux measurements (IH runs), and concentrations of $^4$He. The relative error of the measured $^4$He concentration was well within 5%. The $^4$He analytical blank was within $4.5 \times 10^{-14}$ mol. The blank incremental heating runs have proven to be negligible compared to any curve obtained for a sample.

U and Th were determined via the ICP-MS method using a quadrupole mass-spectrometer ELAN-DRC-6100 in the Karpinsky Russian Geological Research Institute (St. Petersburg, Russia). The relative error of element determination did not exceed 5%–10%.

### *3.3. Data Processing*

The input data (helium release patterns) were represented by a two-line array (time–intensity). The temperature was read every 50–100° depending on the heating rate and inserted into the record as reference points, which were hereafter used to re-calculate the data into an temperature–intensity array. The linearity of the temperature ramp was additionally controlled by a record of readings of the measuring thermocouple.

It was assumed that the recorded ion current is proportional to the $^4$He flux through the chamber, which means that the area under the curve is proportional to the helium amount. Complex curves were approximated by a set of theoretical peaks to reproduce the experimental curve as accurately as possible. The contribution of each peak to the total helium budget was calculated as a fraction of the area of this peak in the total area of the curve.

It was also assumed that the sample was represented by a set of sphere-shaped particles of the same (unknown) radius, and that diffusion coefficient $D$ was controlled by the Arrhenius equation:

$$D = D_0 \exp(-E/RT)$$

where $D_0$—the frequency factor representing diffusion coefficient at infinitely high temperature, $E$—the activation energy, $T$—the temperature.

The mechanism adopted for helium release from the crystalline matrix was volume diffusion [24]:

$$\frac{\partial C}{\partial t} = D\left(\frac{2}{r}\frac{\partial C}{\partial r} + \frac{\partial^2 C}{\partial r^2}\right)$$

where $D$ is the diffusion coefficient, $C$ is the concentration, and $r$ is the position. The initial and boundary conditions specify that the initial concentration $C_0$ is constant throughout the sample and that, at the sample boundary, it drops to zero.

Solving the equation by taking into account initial and boundary conditions, we obtain the following equation:

$$C = -C_0 \frac{2a}{\pi r} \sum_{n=1}^{\infty} \frac{(-1)^n}{n} \exp\left(-\frac{n^2\pi^2}{a^2} \int_0^t D dt'\right) \sin\left(\frac{n\pi}{a} r\right) \quad (1)$$

Then, for the relative amount of released gas:

$$\begin{aligned} \overline{M} &= 1 - \frac{\int_0^a 4\pi r^2 C dr}{\int_0^a 4\pi r^2 C_0 dr} \\ &= 1 - \frac{6}{\pi^2} \sum_{n=1}^{\infty} \frac{1}{n^2} \exp\left(-\frac{n^2\pi^2}{a^2} \int_0^t D dt'\right) \\ &= 1 - \frac{6}{\pi^2} \sum_{n=1}^{\infty} \frac{1}{n^2} \exp\left(-\frac{n^2\pi^2 D_0}{a^2 dT/dt} \cdot \left(\frac{E}{R}\mathrm{Ei}\left(-\frac{E}{RT}\right) + T\exp\left(-\frac{E}{RT}\right) - \frac{E}{R}\mathrm{Ei}\left(-\frac{E}{RT_0}\right) - T_0\exp\left(-\frac{E}{RT_0}\right)\right)\right) \end{aligned}$$

where $T_0$ is the initial temperature of the run, and Ei is the exponential integral function. The normalized helium flux intensity:

$$\begin{aligned} \overline{F} &= \frac{d\overline{M}}{dt} \\ &= \frac{6D}{a^2} \sum_{n=1}^{\infty} \exp\left(-\frac{n^2\pi^2}{a^2} \int_0^t D dt'\right) \\ &= \frac{6D_0}{a^2} \exp\left(-\frac{E}{RT}\right) \sum_{n=1}^{\infty} \exp\left(-\frac{n^2\pi^2 D_0}{a^2 dT/dt} \cdot \left(\frac{E}{R}\mathrm{Ei}\left(-\frac{E}{RT}\right) + T\exp\left(-\frac{E}{RT}\right) - \frac{E}{R}\mathrm{Ei}\left(-\frac{E}{RT_0}\right) - T_0\exp\left(-\frac{E}{RT_0}\right)\right)\right), \end{aligned}$$

where $R$—the universal gas constant, $E$—the activation energy, $a$—the radius of sample particles.

The closure temperature ($T_c$) was defined by Dodson [25] as follows:

$$\frac{E}{RT_c} = \ln\left(-\frac{ART_c^2 D_0/a^2}{EdT/dt}\right),$$

where $A$—the shape constant, $dT/dt$—the cooling rate.

Solving the equation gives the formula for $T_c$:

$$T_c = \frac{E}{2R} W_0\left(\sqrt{-\frac{1}{4}\frac{AED_0/a^2}{RdT/dt}}\right)^{-1},$$

where $W_0$—the Lambert W function.

For our calculations, we take $A$ = 55, meaning spherical inclusions, and $dT/dt$ = −100 K/Ma.

The above theory was used to create software intended to generate synthetic peaks of diffusion-driven helium release and to calculate diffusion parameters ($E$, $D_0/a^2$), closure temperatures, and a portion of extracted helium corresponding to the given peak.

Since the curve-fitting algorithm for approximating the complex curve by two or more theoretical peaks has failed in several cases, we secured an option of manual fitting. The number of the peaks was kept to a minimum: another peak was added only when its presence was obvious. Variable peak parameters were height, width, position on the temperature scale, and the approximation of volume diffusion, i.e., number of terms in the sum (1). The latter could take the values from 1 to 50; when the parameter takes the value 1, the diffusion mechanism is reduced to first-order reaction kinetics. All parameters were chosen so that, to minimize the discrepancy between the observed and synthetic curve,

they were then recalculated into the control parameters ($E$ and $D_0/a^2$). The relative error of the control parameter $a_j$ was calculated using the formula

$$\delta_{a_j} = \frac{1}{a_j}\sqrt{\frac{f\left(a_{fit}\right)}{N-M}\left|H_{jj}^{-1}\right|} \quad (2)$$

where $f$—the quadratic loss function, $N$—the number of data points, $M$—the number of parameters, $H$—the Hessian matrix. This assumes that data follow the given model and residuals are normally distributed.

## 4. Results

The available collection of the Salla-Kuolajarvi rocks offered a rather limited number of potentially suitable samples. The oxide and sulfide minerals (magnetite, hematite, and pyrite), as well as amphibole, were the only minerals selected in sufficient quantities to try out the proposed methodological protocol. Iron oxides have previously been used in this capacity, especially hematite, which was found to be a promising thermochronometer [26–28], despite the wide variation in the closure temperature estimates. The apparent U-Th-He age obtained for the amphibole of the Ponoi Massif [29] indicated good helium preservation in this mineral. In recent years, there were also reportedly successful attempts to date pyrite [30]. Rock-forming minerals like feldspars and quartz were rejected as obviously unpromising for studying the U-Th-He system. The results of processing runs are summarized in the Table 1.

### *4.1. Pyrite*

The two studied pyrite samples (KR-3 and KR-153) show, in general, similar patterns of He release. The patterns obtained for the two fractions of the sample KR-3 are presented in Figure 3. The comparison of the kinetics of helium release from grains (Figure 3a) and ground pyrite (Figure 3b) indicates that the dominant peak reflects inclusion-hosted helium trapped from the mineral-forming medium; the analysis of the overall helium budget indicates that about 90% of the trapped helium was released during sample grinding. Moreover, this peak is confined to exactly the same temperature (~600°) in the both images, which is indicative of decrepitation rather than of diffusive loss. Otherwise, the helium flow from the unground sample was perceptibly higher than the blank run starting from the temperature as low as 250 °C forming a sequence of weakly resolved peaks, which may or may not be diffusive. An attempt to approximate those with one wide diffusive peak resulted in a very low closure temperature (see Table 2). Since the amount of trapped helium in the pyrite grains overshadows any radiogenic input, we used a ground sample to estimate the age, and used two presumably diffusive peaks (colored green and blue in Figure 3b) for the corrected age. The two-peak approximation of the seemingly uniform hump was used because of its distinctly (and inversely) asymmetric shape, which counters the very nature of diffusion and makes the approximation by a single diffusion peak very rough. In addition, the blue peak seems to have a counterpart in Figure 3a, while the green one might have been overlapped by the prevailing decrepitation process. Each of these peaks corresponds to a higher closure temperature (also shown in Table 2), which may be accountable for the presence of some radiogenic helium in these samples. The estimated U-Th-He dates, however, are very vague, due to both the overwhelming amount of the trapped helium, the indefinite nature of individual peaks, and the superposition of the peaks on the temperature scale. They do not correspond to any previously known date; also, some partial loss of the radiogenic helium may have occurred during grinding.

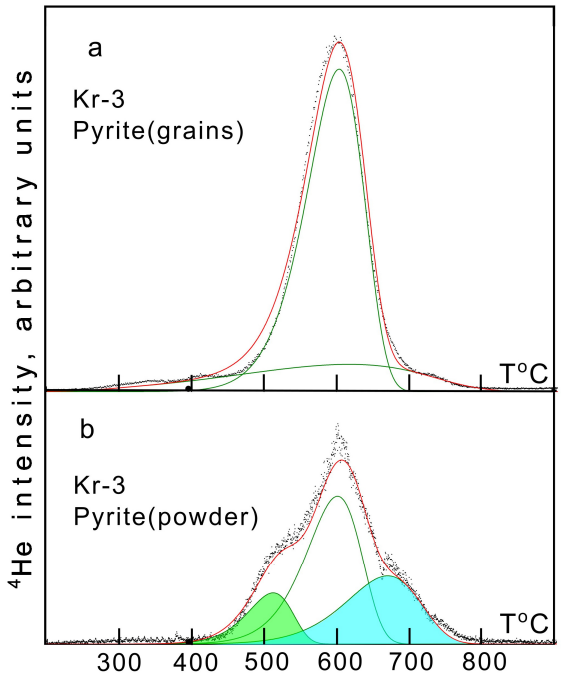


**Figure 3.** The patterns of helium IH release from the pyrite sample KR-3. Black dots are experimental data, green lines denote individual approximating peaks, while the red line is a sum of the approximating peaks. (**a**) IH of the grain fraction; (**b**) IH of the sample ground in agate mortar. Colored peaks were assumed radiogenic and used for the calculation of the corrected age.

**Table 2.** Measured U, Th, and He concentrations and parameters inferred from IH patterns of 4He release.

| Sample | U | Th | $^4$He | Bulk Age | Corr. Age * | $E_a$ ** | $D_0/r^2$ ** | Closure T |
|---|---|---|---|---|---|---|---|---|
| | ppm | ppm | μmole × kg$^{-1}$ | Ma | Ma | kJ | s$^{-1}$ | °C |
| KR-3 *** Pyrite | 0.57 | 0.76 | 1.09 | 270 | 154 | 75.5 (0.3)/ 138 (0.1) | $2.9 \times 10^1$ (3.4)/ $5.4 \times 10^4$ (2.4) | −15–30/ 109 |
| KR-13 Magnetite | 1.01 | 3.25 | 14.73 | 1534 | – | 144.2 (0.1) | $2.4 \times 10^3$ (1.1) | 140–160 |
| KR-77 Hematite | 0.56 | 0.38 | 5.80 | 1661 | 1874 | 101 (0.2) and 255.5 (<0.1) | $1.4 \times 10^2$ (3.6) and $3.2 \times 10^7$ (0.4) | 55–75 and ~340 |
| KR-82 Hornblende | 0.24 | 0.99 | 10.36 | 4055 | 3357 | 72.0 (0.1) | $8.6 \times 10^0$ (1.0) | 15–40 |
| KR-118 Magnetite | 1.32 | 0.44 | 0.15 | 20 | 16 | 147.6 (<0.1) | $1.56 \times 10^4$ (0.9) | 175 |
| KR-153 Pyrite | 7.93 | 0.38 | 3.49 | 81 | 5.32 | ~70 (0.7) | $1.15 \times 10^0$ (3.4) | −20–0 |

* The corrected age is the age calculated from the bulk contents of U and Th, and the in situ-produced helium portion, quantified from IH patterns by means of the geometric approach described above. ** Relative approximation errors calculated according to the Equation (2) are given in brackets (per cent). *** Age values were obtained from ground samples using the peak layout shown in Figure 3b. Other parameters were calculated from the coarse fraction under the assumption that the diffusive loss had occurred in a single broad peak, as in Figure 3a/for the blue peak in Figure 3b.

### *4.2. Amphibole*

The pattern of helium release from amphibole concentrate (magnesian hornblende, sample KR-82) forms two almost completely resolved peaks of regular shape, one of which reaches a maximum at 630 °C and represents helium diffusion from the amphibole crystalline matrix (Figure 4). The nature of the second peak (930°) is still unclear. It could be primary fluid inclusions or a specific position in the lattice [31]. Either way, it is absent

from the ground sample. Such helium release patterns are characteristic of amphibole [8]; it was also believed that helium preservation in this mineral is quite good. Thus, the work in [29] reported a more or less accurate Proterozoic date inferred by the U-Th-He system in the amphibole. The closure temperature for the radiogenic helium determined from the parameters of this peak is, however, rather low (see Table 2). At the same time, the apparent age, even without taking into account the contribution of the high-temperature peak, indicates a huge helium excess which, presumably, reflects the ability of amphibole (or at least this particular variety) to capture helium from the mineral-forming medium directly into the structure/structure defects, without the formation of fluid inclusions as a separate phase. This conclusion is also supported by invariable shape of the He-release pattern: though the high-temperature peak may by absent, no other than the two mentioned above are ever present. The evident excess of helium combined with rather low closure temperature may have been due to several reasons: (i) if the actual value of the closure temperature lies within the assessed temperature range, the helium budget is a result of partial helium loss, which means that the initial excess was even bigger; (ii) the assessed diffusivity might be overestimated either due to incorporation of smaller peak into the larger one and respective distortion of the peak shape, or as a result of a discrepancy between the theoretical model and actual degassing. In any case, this phenomenon is beyond the scope of the present study, but as a conclusion, the amphibole formed in the fluid-rich setting seems to be useless for U-Th-He dating.

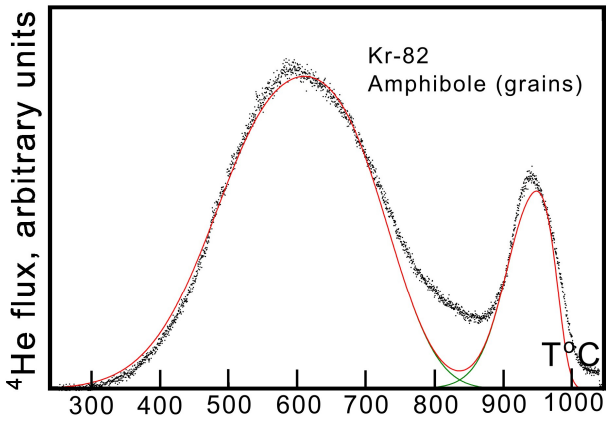


**Figure 4.** The pattern of helium IH release from the amphibole sample KR-82 black dots—experimental data; green lines—individual approximating peaks; red line—sum of the approximating peaks.

### *4.3. Magnetite*

The incremental heating curves obtained for two magnetite concentrates are shown in Figure 5a,b. In one of the studied samples (KR-118), two pronounced, although not fully resolved, peaks were observed within the studied temperature range. In the other (KR-13), the helium release was outside the operating temperature range of the incremental heating experiment (1050 °C), although in both cases there is clearly a second helium peak. The high-temperature peak presumably corresponds to the helium of fluid inclusions since its characteristic temperature was not affected by the heating rate. Slowing down the heating rate twice made another (lower-temperature) peak shift by ~30 °C, which made it appear diffusive. An incomplete pattern, however, made geometric age correction ambiguous, as shown in Figure 5a. The helium concentrations determined in the two samples apparently present an explanation for differences in IH curves, while the apparent age of sample KR-13 shows that the U-Th-He system within the mineral was reset at some point after formation of chlorite and carbonate metasomatic rocks after albitite 1.62 Ga ago [23] and undisturbed during later known events, whereas that of KR-118 is well within 20 Ma. This difference may be due to the fact that the magnetite in sample KR-13 is primary and associated with

the formation of plagioshale, whereas magnetite in sample KR-118 is confined to secondary biotite accumulations and is associated either with recrystallization processes or was altered during these processes. Curiously, however, the diffusion parameters inferred from the both samples are close; this fact calls for further investigation. IH patterns of the ground samples are shown on the same plots (not to scale) as respective coarser fractions. While the peaks of KR-118 powder are just shifted along the temperature scale, the grinding of the KR-13 sample cannot be regarded as merely reducing particle size; the two additional peaks may reflect some processes occurring during heating that have been enhanced by sample grinding. The value of the closure temperature of the U-Th-He system obtained for the two samples is stable and rather high (~150°), however, it is still lower than the published estimate [32]. This fact, as well as the realistic (although yet to be confirmed using either similar samples or repeated experiments) age value obtained for sample KR-13, imply that magnetite is a promising material for exercising the IH approach to obtaining U-Th-He age constraints.

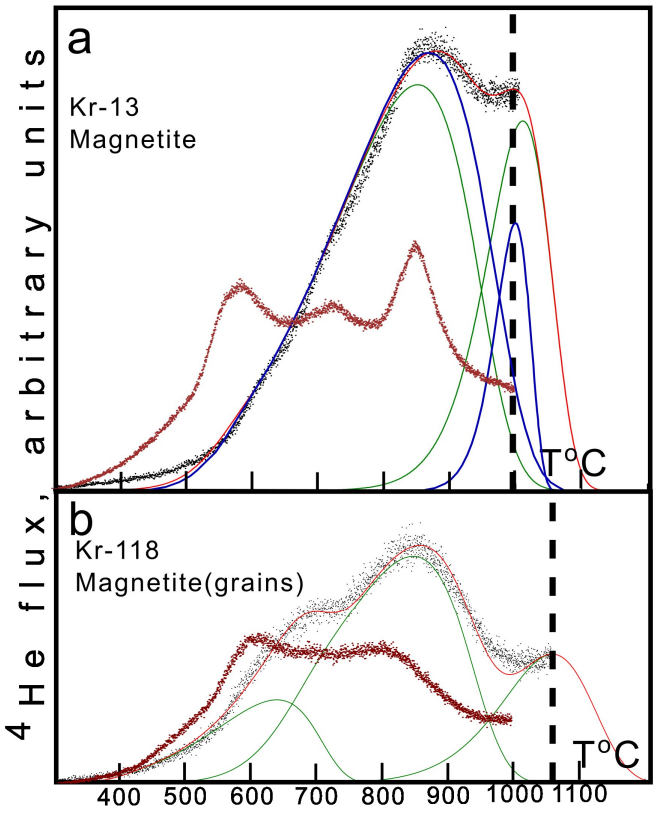


**Figure 5.** The patterns of helium IH release from the magnetite samples; (**a**)—sample KR-13, (**b**)—KR-118. Black dots—experimental data (grains); purple dots—experimental data (ground sample). The two patterns are not to scale. Dashed lines denote the end of IH patterns for grains; green and blue lines—individual approximating peaks; red line—sum of the approximating peaks. The green and blue contours on Figure 5a are two possible options to represent the same incomplete pattern as a sum of two peaks. Table 2 presents the respective range of apparent age values.

### *4.4. Hematite*

To obtain the helium release curve from sample KR-77 (hematite concentrate, Figure 6a), we had to slow down the linear heating rate by a factor of 2 (the initial pattern is shown in Figure 6b; such a measure allowed us to register two helium peaks that are approximated by the theoretical curves and, accordingly, are sufficiently well separated geometrically). The closure temperature of the low-temperature peak (~65 °C) is significantly lower than that of magnetite, however, it is still somewhat higher than the ambient temperature on the Earth's surface, hence it allows a meaningful interpretation. The higher-

temperature hump also seems to correspond to diffusive helium loss: (i) the lower IH rate made it shift down the temperature scale; (ii) the sample grinding did not much affect the helium release pattern. The estimated closure temperature of this peak (~350 °C), as far as we know, exceeds any assessments previously made for hematite [33,34]. Such a pattern may have resulted from the degassing of some impurity mineral, although the only viable candidate among the selection of impurities (quartz, albite, clinochlore, biotite, gypsum) was biotite (3.2%), however, it is also possible that this is an inherent pattern of the hematite. The total helium budget reveals good the preservation of radiogenic helium, and apparent age is close to the estimated uraninite age obtained earlier.

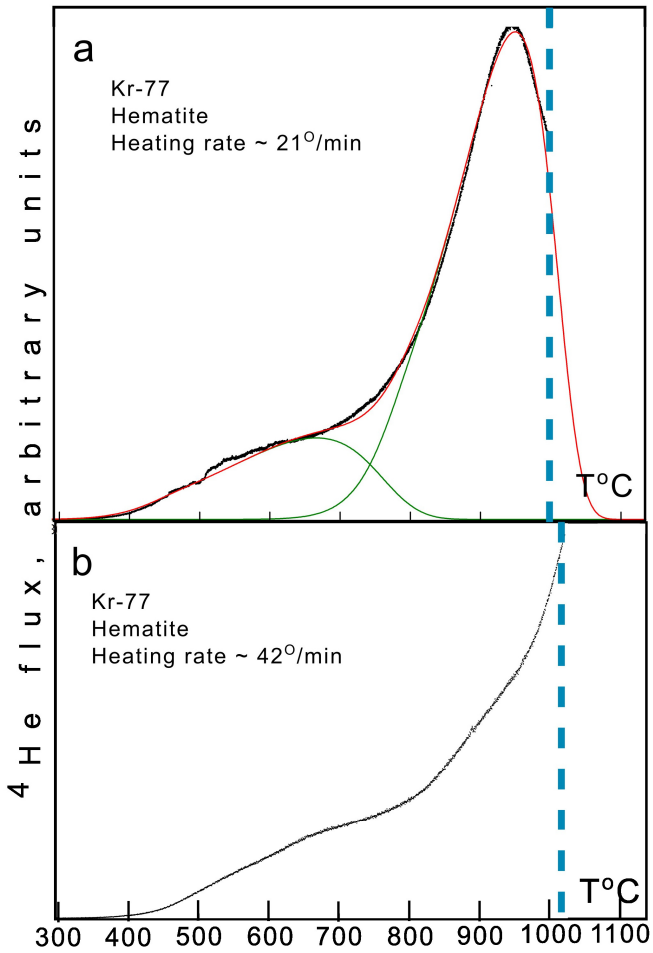


**Figure 6.** The pattern of helium IH release from the hematite sample KR-77. Black dots—experimental data; dashed line denotes end of IH experiment; green lines—individual approximating peaks; red line—sum of the approximating peaks; (**a**) IH at a rate of 21° per min; (**b**) IH at a rate of 42° per min.

## 5. Discussion

The new approach to the separation of the trapped and produced in situ helium components and mobility estimates for the latter is based on the concept of "sites" of a different nature within the mineral, which, on the sufficiently short experimental scale, can be treated as independent. The above results indicated that it is not always so: it turned out that excess helium in the amphibole is released at the same time with a radiogenic component. It was also shown that some samples, like pyrite, may produce virtually unreadable IH patterns because of a high proportion of the trapped helium overlapping with the peak of radiogenic helium. Thus, iron oxides (magnetite and especially hematite), already known as solid thermochronometers, are still the best hope for obtaining meaningful chronological constraints for this particular object.

As was inferred from the IH pattern obtained from the sample KR-118, some magnetite varieties may be altered to the extent when they are not able to quantitatively preserve helium over geological time. The connection between the nature of the specific alteration processes and helium diffusivity is yet to be explored, yet it is clear that the altered mineral retained its crystal structure enough to be identified by X-ray diffractometry as magnetite. However, there may also be another explanation, especially since the pyrite sample KR-153, has shown a similar age of several Ma (see Table 2). Neither of the closure temperatures was very high, therefore, provided these samples were by that time on the surface, they might have been corrupted, e.g., by forest fire.

The diffusion parameters/closure temperatures were reported earlier for both magnetite [32] and hematite [33,34]. Our results are reasonably close to those values, however, the Tc we obtained for magnetite was lower than any published value; the temperature obtained for hematite, on the contrary, is higher. As the method is novel, both the model and experimental procedure are probably in for improvements, however, the IH patterns presented in Figures 5 and 6 present a perfectly logical explanation for such a discrepancy. The peak of radiogenic helium in magnetite is closely followed by the release of the better retained fluid inclusions, while hematite has a two-hump pattern of diffusive helium release. If such are common patterns for those minerals, then the conventional approach (stepwise heating) to assessing diffusivity would mix these two peaks and produce intermediate results: a higher mobility for hematite and better retention for magnetite.

Thus, the diffusion parameters as well as closure temperatures obtained for radiogenic helium in various minerals appear mostly realistic in spite of the rather simple model, with no account taken for such matters as the distribution of the diffusion radii or the shape of the sample particles. Later versions of the model are bound to be more intricate. In addition, they are to be calibrated against any data available, such as the independently assessed coarseness of the sample, the different isotopic composition of trapped and radiogenic helium, age data, etc.

The geometric separation of peaks may be quite effective, however, as was shown by both pyrite and magnetite, the incompletely resolved peaks sometimes allow for ambiguous interpretation. The situation might yet improve when more information about the behavior of specific mineral species is available. Nevertheless, the ambiguity is an inherent feature of inverse problems, and this poses another problem: the resulting reliability estimate of the data obtained should somehow combine experimental errors with accuracies of both the model and approximation. We have so far only evaluated the influence of discrepancy between theoretical and experimental patterns onto the diffusion parameters, which is, of course, not enough.

It should be stressed that the method proposed, at least at the present state, cannot provide accurate thermochronological data. It does, however, give an idea of the ratio of trapped and radiogenic in situ-produced helium and of the mobility of the latter—all of that in a single experiment. Thus, the approach definitely deserves further efforts.

## 6. Conclusions

The following preliminary conclusions can be made:

(1) Despite the fact that the studied minerals have a metasomatic origin and structures, the actual preservation of helium, e.g., in iron oxides, allows us to count on obtaining significant chronological information.

(2) The geometric method for separating trapped and radiogenic helium has been used for the first time; it needs both verification (calibration) using a priori data and improvement. In particular, IH experiments should be performed up to the complete degassing of the sample, which is sometimes confined to the sample fusion temperature.

(3) Since the proposed approach imposes very few restrictions on the material investigated, processing several samples formed under similar conditions and/or a repeated experiment would be advisable. Such a practice should give an indication of the reliability of age estimates.

(4) The technique proposed may just as well be used for the more accurate quantification of the trapped component. Such an application may prove even more effective in cases where contrast isotopic signatures of the two components are expected.

**Author Contributions:** Conceptualization, M.A.G. and T.V.K.; methodology, M.A.G., A.E.G. and V.V.K.; software, A.E.G.; geological background, A.A.K.; writing—original draft preparation, M.A.G. and A.A.K.; writing—review and editing, M.A.G., A.A.K. and T.V.K.; visualization, M.A.G. and T.V.K. All authors have read and agreed to the published version of the manuscript.

**Funding:** The work was carried out with the aid of the Russian Scientific Foundation, grant No. 23-27-00416.

**Data Availability Statement:** The original contributions presented in this study are included in the article. Further inquiries can be directed to the corresponding author.

**Acknowledgments:** The authors are grateful to three anonymous reviewers for their comments that helped to substantially improve the manuscript.

**Conflicts of Interest:** The authors declare no conflicts of interest.

## References

1. Zeitler, P.K.; Herczig, A.L.; McDougall, I.; Honda, M. U-Th-He dating of apatite: A potential thermochronometer. *Geochim. Cosmochim. Acta* **1987**, *51*, 2865–2868. [CrossRef]
2. Farley, K.A. (U-Th)/He dating: Techniques, calibrations, and applications. *Rev. Mineral. Geochem.* **2002**, *47*, 819–844. [CrossRef]
3. Flowers, R.M.; Zeitler, P.K.; Danišík, M.; Reiners, P.W.; Gautheron, C.; Ketcham, R.A.; Metcalf, J.R.; Stockli, D.F.; Enkelmann, E.; Brown, R.W. (U-Th)/He chronology: Part 1. Data, uncertainty, and reporting. *GSA Bull.* **2023**, *135*, 104–136. [CrossRef]
4. Ault, A.K.; Gautheron, C.; King, G.E. Innovations in (U–Th)/He, fission track, and trapped charge thermochronometry with applications to earthquakes, weathering, surface-mantle connections, and the growth and decay of mountains. *Tectonics* **2019**, *38*, 3705–3739. [CrossRef]
5. Farley, K.A.; Wolf, R.A.; Silver, L.T. The effects of longalpha-stopping distances on (U–Th)/He ages. *Geochim. Cosmochim. Acta* **1996**, *60*, 4223–4229. [CrossRef]
6. Murray, K.E.; Orme, D.A.; Reiners, P.W. Effects of U–Th-rich grain boundary phases on apatite helium ages. *Chem. Geol.* **2014**, *390*, 135–151. [CrossRef]
7. Ketcham, R.A.; Gautheron, C.; Tassan-Got, L. Accounting for long alpha-particle stopping distances in(U–Th–Sm)/He geochronology: Refinement of the base-line case. *Geochim. Cosmochim. Acta* **2011**, *75*, 7779–7791. [CrossRef]
8. Tolstikhin, I.; Tarakanov, S.; Kolobov, V.; Gannibal, M. Mobility of Radiogenic Helium in Amphibole. *Minerals* **2021**, *11*, 27. [CrossRef]
9. Gerling, E.K. *Current State of the Argon Method for Determining Age and Its Application in Geology*; Publishing House of the USSR Academy of Sciences: Saint Petersburg, Russia, 1961. (In Russian)
10. Levskii, L.K. Diffusion of helium from stony meteorites. *Geochemistry* **1963**, *6*, 556–561.
11. Fechtig, H.; Kalbitzer, S. The diffusion of argon in potassium-bearing solids. In *Potassium–Argon Dating*; Schaefer, O.A., Zahringer, J., Eds.; Springer: Berlin/Heidelberg, Germany, 1966; pp. 68–107.
12. Tolstikhin, I.; Kamensky, I.; Tarakanov, S.; Kramers, J.; Pekala, M.; Skiba, V.; Gannibal, M.; Novikov, D. Noble gas isotope sites and mobility in mafic rocks and olivine. *Geochim. Cosmochim. Acta* **2010**, *74*, 1436–1447. [CrossRef]
13. McDannell, K.; Zeitler, P.; Janes, D.; Idleman, B.; Fayon, A. Screening apatites for (U-Th)/He thermochronometry via continuous ramped heating: He age components and implications for age dispersion. *Geochim. Cosmochim. Acta* **2018**, *223*, 90–106. [CrossRef]
14. Idleman, B.D.; Zeitler, P.K.; McDannell, K.T. Characterization of helium release from apatite by continuous ramped heating. *Chem. Geol.* **2018**, *476*, 223–232. [CrossRef]
15. Guo, H.; Zeitler, P.K.; Bruce, D.; Idleman, B.; Fayon, A.; Fitzgerald, P.G.; McDannell, K.T. Helium diffusion systematics inferred from continuous ramped heating analysis of Transantarctic Mountains apatites showing age overdispersion. *Geochim. Cosmochim. Acta* **2021**, *310*, 113–130. [CrossRef]
16. Tolstikhin, I.N.; Kamensky, I.L.; Marty, B.; Nivin, V.A.; Vetrin, V.R.; Balaganskaya, E.G.; Ikorsky, S.V.; Gannibal, M.A.; Weiss, D.; Verhulst, A.; et al. Rare gas isotopes and parent trace elements in ultrabasic-alkaline-carbonatite complexes, Kola Peninsula: Identification of lower mantle plume component. *Geochim. Cosmochim. Acta* **2002**, *66*, 881–901. [CrossRef]
17. Kalinin, A.A. Tellurium and Selenium Mineralogy of Gold Deposits in Northern Fennoscandia. *Minerals* **2021**, *11*, 574. [CrossRef]
18. Kulikov, V.S.; Kulikova, V.V. The Kuolajarvi synclinorium: A new view on the geological structure and combined cross section. In *Trudy Karel'skogo Nauchnogo Tsentra RAN*; Karel'skiy Nauchniy Tsentr RAN: Petrozavodsk, Russia, 2014; pp. 28–38. (In Russian)
19. Hölttä, P.; Heilimo, E.; Huhma, H.; Kontinen, A.; Mertanen, S.; Mikkola, P.; Paavola, J.; Peltonen, P.; Semprich, J.; Slabunov, A.; et al. *The Archaean of the Karelia Province in Finland*; Special Paper 54; Geological Survey of Finland: Espoo, Finland, 2012; pp. 21–73.

20. Kalinin, A.A. Stages of Gold Deposits Formation in the Precambrian of the North-Eastern Fennoscandia. *Minerals* **2022**, *12*, 537. [CrossRef]
21. Kalinin, A.A. *Gold in Metamorphic Complexes of the North-Eastern Part of the Fennoscandian Shield*; Federal Research Centre 'Kola Science Centre': Apatity, Russia, 2018; 250p. (In Russian)
22. Kalinin, A.A.; Kaulina, T.V.; Lyalina, L.M.; Elizarov, D.V.; Serov, P.A. Stages in the formation of uranium mineralization in the Salla-Kuolajarvinskaya zone (Northern Karelia): Geological and isotope geochronological data. *Geol. Ore Depos.* **2016**, *58*, 594–599. [CrossRef]
23. Safonov, Y.G.; Volkov, A.V.; Volfson, A.A.; Genkin, A.D.; Krylova, T.L.; Chugaev, A.V. The Mayskoye gold-quartz deposit, Northern Karelia: Geological and mineralogical-geochemical peculiar features and genesis issues. *Geol. Ore Depos.* **2003**, *45*, 429–451.
24. Crank, J. *The Mathematics of Diffusion*, 2nd ed.; Clarendon Press: Oxford, UK, 1975; 414p.
25. Dodson, M.H. Closure temperature in cooling geochronological and petrological systems. *Contrib. Mineral. Petrol.* **1973**, *40*, 259–274. [CrossRef]
26. Ault, A.K.; Frenzel, M.; Reiners, P.W.; Woodcock, N.H.; Thomson, S.N. Record of paleofluid circulation in faults revealed by hematite (U-Th)/He and apatite fission-track dating: An example from Gower Peninsula fault fissures, Wales. *Lithosphere* **2016**, *8*, 379–385. [CrossRef]
27. Evenson, N.S.; Reiners, P.W.; Spencer, J.; Shuster, D.L. Hematite and Mn oxide (U-Th)/He dates from the Buckskin-Rawhide detachment system, western Arizona: Constraining the timing of mineralization and hematite (U-Th)/He systematics. *Am. J. Sci.* **2014**, *314*, 1373–1435. [CrossRef]
28. Farley, K.A.; McKeon, R.E. Radiometric dating and temperature history of banded iron formation-associated hematite, Gogebic iron range, Michigan, USA. *Geology* **2015**, *43*, 1083–1086. [CrossRef]
29. Tolstikhin, I.N.; Verchovsky, A.B.; Kamensky, I.L.; Skiba, V.I.; Gannibal, M.A.; Vetrin, V.R.; Tarakanov, S.V. Amphibole: A major carrier of helium isotopes in crustal rocks. *Chem. Geol.* **2016**, *444*, 187–198. [CrossRef]
30. Yakubovich, O.V.; Podolskaya, M.M.; Vikentiev, I.V.; Fokina, E.L.; Kotov, A.B. U-Th-He geochronology of pyrite from the Uzelga VMS deposit (Urals): New perspectives for direct dating of the ore-forming processes. *Minerals* **2020**, *10*, 629. [CrossRef]
31. Jackson, C.R.M.; Shuster, D.L.; Parman, S.W.; Smye, A.J. Noble gas diffusivity hindered by low energy sites in amphibole. *Geochim. Cosmochim. Acta* **2016**, *172*, 65–75. [CrossRef]
32. Blackburn, T.J.; Stockli, D.F.; Walker, J.D. Magnetite (U-Th)/He dating and its application to the geochronology of intermediate to mafic volcanic rocks Earth Planet. *Sci. Lett.* **2007**, *259*, 360–371.
33. Bahr, R.; Lippolt, H.J.; Wernicke, R.S. Temperature-induced 4He degassing of specularite and botryoidal hematite: A 4He retentivity study. *J. Geophys. Res.* **1994**, *99*, 17695–17707. [CrossRef]
34. Wernicke, R.S.; Lippolt, H.J. Botryoidal hematite from the Schwarzwald (Germany): Heterogeneous uranium distributions and their bearing on the helium dating method. *Earth Planet. Sci. Lett.* **1992**, *114*, 287–300. [CrossRef]


**Disclaimer/Publisher's Note:** The statements, opinions and data contained in all publications are solely those of the individual author(s) and contributor(s) and not of MDPI and/or the editor(s). MDPI and/or the editor(s) disclaim responsibility for any injury to people or property resulting from any ideas, methods, instructions or products referred to in the content.